Role of the K-Channel in the pH-Dependence of the Reaction of Cytochrome *c* Oxidase with Hydrogen Peroxide†

Catherine Pecoraro,‡ Robert B. Gennis,*,‡ T. V. Vygodina,§ and A. A. Konstantinov*,§

Department of Biochemistry, University of Illinois, Urbana, Illinois 61801, and A. N. Belozersky Insitute of Physico-Chemical Biology, Moscow State University, Moscow, Russia

Received January 18, 2001

ABSTRACT: The reaction of cytochrome *c* oxidase (COX) from *Rhodobacter sphaeroides* with hydrogen peroxide has been studied at alkaline (pH 8.5) and acidic (pH 6.5) conditions with the aid of a stopped-flow apparatus. Absorption changes in the entire 350−800 nm spectral range were monitored and analyzed by a global fitting procedure. The reaction can be described by the sequential formation of two intermediates analogous to compounds I and II of peroxidases: oxidized COX + H_2O_2 → intermediate I → intermediate II. At pH as high as 8.5, intermediate I appears to be a mixture of at least two species characterized by absorption bands at ∼607 nm (**P**$_{607}$) and ∼580 nm (**F-I**$_{580}$) that rise synchronously. At acidic pH (6.5), intermediate I is represented mainly by a component with an α-peak around 575 nm (**F-I**$_{575}$) that is probably equivalent to the so-called **F•** species observed with the bovine COX. The data are consistent with a pH-dependent reaction branching at the step of intermediate I formation. To get further insight into the mechanism of the pH-dependence, the peroxide reaction was studied using two mutants of the *R. sphaeroides* oxidase, K362M and D132N, that block, respectively, the proton-conducting K- and D-channels. The D132N mutation does not affect significantly the **Ox** → intermediate I step of the peroxide reaction. In contrast, K362M replacement exerts a dramatic effect, eliminating the pH-dependence of intermediate I formation. The data obtained allow us to propose that formation of the acidic form of intermediate I (**F-I**$_{575}$, F•) requires protonation of some group at/near the binuclear site that *follows* or is concerted with peroxide binding. The protonation involves specifically the K-channel. Presumably, a proton vacancy can be generated in the site as a consequence of the proton-assisted heterolytic scission of the O−O bond of the bound peroxide. The results are consistent with a proposal [Vygodina, T. V., Pecoraro, C., Mitchell, D., Gennis, R., and Konstantinov, A. A. (1998) *Biochemistry 37*, 3053−3061] that the K-channel may be involved in the delivery of the first four protons in the catalytic cycle (starting from reduction of the oxidized form) including proton uptake coupled to reduction of the binuclear site and transfer of protons driven by cleavage of the dioxygen O−O bond in the binculear site. Once peroxide intermediate I has been formed, generation of a strong oxene ligand at the heme a_3 iron triggers a transition of the enzyme to the "peroxidase conformation" in which the K-channel is closed and the binuclear site becomes protonically disconnected from the bulk aqueous phase.

Cytochrome oxidase (COX) is a key respiratory enzyme that reduces molecular oxygen to water and conserves the free energy of this exergonic reaction in the form of an electrochemical potential difference of H^+ ions across the coupling membrane of mitochondria or bacteria (*1*, *2*). This process involves vectorial translocation of protons across the membranes and is often referred to as proton pumping.

The previous decade has been marked by considerable progress in the studies of COX, mainly through the use of site-directed mutagenesis (*3*, *4*) and X-ray crystallography (*5*−*8*). Now that the structure of cytochrome *c* oxidase has been solved with near atomic resolution, the molecular mechanism of the enzyme action as a proton pump has become the issue of primary interest. A provisional scheme of the catalytic cycle of COX is shown in Figure 1, in which the redox state of the heme a_3 iron is depicted.

As pointed out in refs *9* and *10*, the catalytic cycle is comprised of two halves with quite different chemistries, denoted as the *eu-oxidase* and *peroxidase* phases of the reaction. In the eu-oxidase half, the oxidized enzyme is reduced by two electrons, O_2 binds to ferrous heme a_3, and is then reduced to peroxide. The hypothetical intermediate denoted **P**$_0$ in Figure 1, with the ionized peroxide bound to ferric heme a_3, is rapidly converted via the doubly protonated transition state **P**$_0$* (cf. refs *11*−*13*) to a ferryl-oxo species **F**$_1$ to begin the peroxidase phase of the reaction cycle. Nomenclature is adopted to emphasize the similarity of the states of cytochrome oxidase and the intermediates characteristic of peroxidase enzymes: compound 0, compound I, and compound II (*9*, *10*). Hence, the inferred bound peroxide

† Supported by grants from the National Institutes of Health (HL16101) (R.B.G.), a Fogarty International Collaborative Award (TW00349) (R.B.G. and A.A.K.), NATO Collaboration, Grant LST-.CLG. 975851 (R.B.G. and A.A.K.), Civilian Research and Developent Fund Award RC1-2063 (R.B.G. and A.A.K.), Grant 00-04-48251 from the Russian Fund for Basic Research (A.A.K.), and Howard Hughes Medical Institute International Scholar Award 55000320 (A.A.K.).

* To whom correspondence should be addressed.

‡ University of Illinois.

§ Moscow State University.

10.1021/bi010115v CCC: $20.00 © 2001 American Chemical Society
Published on Web 07/17/2001

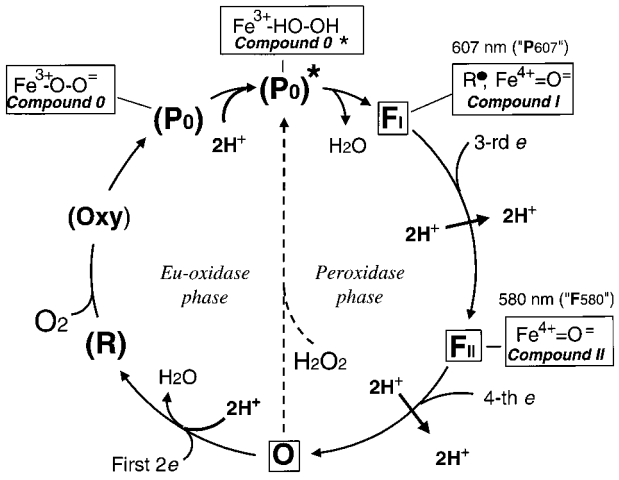

FIGURE 1: Proposed catalytic cycle of cytochrome *c* oxidase, emphasizing division of the reaction into eu-oxidase and the peroxidase halves. Species that are boxed can be experimentally observed; those in brackets denote the states that have not been resolved (the $\mathbf{P}_0$ and $\mathbf{P}_0$***** states) or that have been observed so far only under some specific artificial conditions (**R** and **Oxy**). Four electrogenic phases of intraprotein proton transfer are denoted by thick arrows. The scheme assumes energy coupling of these proton motive steps to four chemical reactions in the cycle: (1) reduction of the binuclear site; (2) proton-assisted splitting of bound peroxide ($\mathbf{P}_0 \rightarrow \mathbf{F}_I$); (3) reduction of compound I-type intermediate to compound II ($\mathbf{F}_I \rightarrow \mathbf{F}_{II}$); (4) reduction of compound II-type intermediate to the ferric oxidized state ($\mathbf{F}_{II} \rightarrow \mathbf{O}$). These phases may not be elementary single-step processes on the time scale of turnover and, importantly, should not be confused (in particular, do not have to be synchronous) with the essentially nonelectrogenic steps of proton uptake (release) from (to) the medium measured as ambient pH changes. The K-channel is proposed to be involved in the electrogenic conduction of the four protons required for formation of two water molecules in the eu-oxidase half of the cycle. The D-channel is involved in the subsequent uptake and electrogenic delivery of four more protons coupled to the peroxidase half-reaction. Specific distribution of the steps at which the protons are released to the outer phase in the peroxidase half-reaction may vary depending on pH, membrane energization, and other conditions. The scheme shows just one of the possibilities. As proton release steps are expected to be much less electrogenic than proton uptake, their location in the catalytic cycle is not so critical for the energy-transduction mechanism of cytochrome *c* oxidase.

states analogous to peroxidase compound 0 are identified with the index "0" ($\mathbf{P}_0$ and $\mathbf{P}_0$*). In the second half of the cycle, the bound peroxide formed transiently in the eu-oxidase phase of the reaction drives a typical peroxidase reaction at the heme a_3 site. This reaction starts with a proton-assisted heterolytic cleavage of the O−O bond and proceeds via two ferryl-oxo intermediates analogous to compound I and compound II of peroxidases and hence denoted as $\mathbf{F}_I$ and $\mathbf{F}_{II}$ in Figure 1. Compound $\mathbf{F}_I$ is an intermediate with an absorption maximum at 607 nm often referred to as "Peroxy" state or $\mathbf{P}_{607}$, while compound $\mathbf{F}_{II}$ corresponds to the conventional "Ferryl" intermediate with a maximum at ∼580 nm in the difference absorption spectrum vs the ferric state. Heterolytic cleavage of the O−O bond and formation of water (transition $\mathbf{P}_0 \rightarrow \mathbf{F}_I$) are accompanied by ferric to ferryl (Fe^{3+} to Fe^{4+}) oxidation of heme a_3, while a modified tyrosine at the enzyme active site is oxidized to a neutral tyrosyl radical (denoted R• in Figure 1) (*14*−*16*).

Some of the intermediates are relatively stable and have been resolved spectroscopically. These are boxed in Figure 1. Other states have not been observed during the normal catalytic cycle but are likely to be formed; these are denoted by brackets in Figure 1. The $\mathbf{O} \rightarrow \mathbf{R}$ and $\mathbf{R} \rightarrow \mathbf{Oxy}$ steps may be thermoneutral or even thermodynamically unfavorable, and it is the last step of the two-electron reduction of O_2 (formation of the putative ferric-peroxy compound $\mathbf{P}_0$ followed by the proton-assisted splitting of the O−O bond) that drives the eu-oxidase half-reaction. Accordingly, this phase may appear as a single concerted reaction under turnover conditions.

Scheme 1

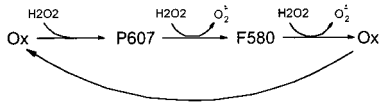

The chemical entities that react with COX in the eu-oxidase half of the cycle ($2H^+$, $2e^-$ and O_2), comprise a molecule of hydrogen peroxide, H_2O_2. Not surprisingly, the reaction of oxidized COX with exogenous H_2O_2 allows one to bypass the eu-oxidase half of the catalytic cycle and to observe a truncated catalytic cycle that includes only the peroxidase phase of the reaction (*17*−*19*) (and see also refs *20* and *21*), as depicted in Figure 1. The reaction of oxidized COX with H_2O_2 can, therefore, be used to generate and characterize the intermediates formed in the peroxidase half-reaction (*10*, *17*, and refs therein).

Despite extensive studies, the mechanism of the interaction of H_2O_2 with oxidized COX is not fully understood. A pseudo-catalase cycle was suggested to describe the H_2O_2 reaction cycle with the oxidized COX at alkaline pH (Scheme 1) (*22*−*24*).

Scheme 1 qualitatively explains some basic features of the reaction, most notably the consecutive generation of compound $\mathbf{P}_{607}$ and compound $\mathbf{F}_{580}$, as well as the formation of superoxide radicals under steady state conditions. However, the process is more complicated as evidenced, in particular, by the characteristics of the same reaction under mildly acidic conditions. As found by Vygodina et al. (*25*, *26*) the yield of the $\mathbf{P}_{607}$ intermediate declines to zero with lowering pH with an apparent p*K* of 6.6. This finding has been confirmed more recently by other workers (*27*, *28*). Detailed kinetic studies of Brittain et al. (*29*) on the peroxide reaction with the cytochrome bo_3 quinol oxidase from *Escherichia coli* and recent work of Junemann et al. on the bovine COX (*28*) provide strong evidence for a pH-dependent branching of the reaction at the level of either the **Ox** or $\mathbf{P}_{607}$ states, and for the formation of at least one more intermediate called either **F′** (*29*, *30*) or **F•** (*28*). Compound **F•** is presumed to be isoelectronic with the $\mathbf{P}_{607}$ state (i.e., two electrons deficient relative to the oxidized enzyme) but is spectroscopically similar to compound $\mathbf{F}_{580}$. Current evidence (*14*, *31*, *32*) strongly indicates that both compound $\mathbf{P}_{607}$ and compound $\mathbf{F}_{580}$ are ferryl-oxo forms of heme a_3 (Figure 1) and, presumably, the same applies to compound **F•** (*33*−*35*).

Experiments with bovine COX reconstituted in phospholipid vesicles have shown that the effect of pH on the peroxide reaction is specifically associated with proton uptake from the matrix (electrically negative) aqueous phase (*25*). This corresponds to the bacterial cytoplasm for the prokaryotic oxidases. The crystal structure of COX reveals two input proton channels connecting the heme-copper redox center

of the enzyme with the electrically negative aqueous phase (reviewed in refs *16* and *36*) which are denoted as the K-channel and the D-channel (*9*). The K-channel is not required for the peroxidase phase of the catalytic cycle, in which the D-channel is utilized (*19*), but it is involved in the delivery of the protons coupled to the reduction of the binuclear center in the eu-oxidase phase of the cycle (*19, 37*−*39*). In addition, it has been proposed that the K-channel may be involved in the uptake of the protons linked to the O−O bond scission at the $\mathbf{P}_0 \rightarrow \mathbf{F}_1$ step (*9, 10, 12, 19*). The current work is motivated to determine the role of the K- and D-channels in the reaction of the enzyme with H_2O_2.

In this work, the reaction of hydrogen peroxide with the oxidized aa_3-type COX from *Rhodobacter sphaeroides* is characterized at both pH 8.5 and pH 6.5. The reactions are compared for the WT enzyme and for two mutants, K362M and D132N, which block, respectively, the K- and D-channels. Rapid mixing techniques were used to initiate the reaction, and the time course was followed by collecting absorption spectra in the entire 350−800 nm range on a time-resolved basis and then analyzed using global fitting. It is known that exposure of COX to mildly acidic pH induces the conversion of the enzyme to a "slow form" that reacts poorly with hydrogen peroxide and other exogenous ligands (*40* and refs therein). Therefore, to avoid this artifact, the reaction of COX with H_2O_2 at pH < 7 was examined using a double-mixing technique so that the enzyme was exposed to acidic pH for just a few seconds prior to initiating the reaction with peroxide.

The results of the study of the wild-type COX from *R. sphaeroides* with peroxide reveal a pH-dependence similar to that described previously for the bovine enzyme. The analysis indicates that peroxide may react along parallel pathways with the protonated and unprotonated forms of the COX, yielding products previously referred to as compound $\mathbf{P}_{607}$ (pH 8.5) or $\mathbf{F}^{\bullet}$ (pH 6.5). A key observation is that the protonation leading to formation of the $\mathbf{F}^{\bullet}$-type product requires the K-channel. Whereas, at weakly alkaline pH the K362M mutant reacts with H_2O_2 in the same way as does the WT enzyme, the mutation eliminates the pH-dependence of the reaction products such that the reaction of K362M with H_2O_2 at pH 6.5 remains essentially the same as at pH 8.5. No such effect is exerted by the D132N substitution in the D-channel. This finding indicates that the group responsible for directing the reaction of COX with H_2O_2 via the formation of species $\mathbf{F}^{\bullet}$ (or $\mathbf{F}$-$\mathbf{I}_{575}$ as denoted in this work) is protonated through the K-channel.

MATERIALS AND METHODS

Chemicals. Hydrogen peroxide was "Suprapur" grade from Merck. The extinction coefficient of 40 M^{-1} cm^{-1} at 240 nm was used to determine the peroxide concentration in the stock solutions after serial dilutions (*41*).

Cell Growth and Purification of the Enzyme. WT and mutant strains of *R. sphaeroides*, all histidine-tagged as previously described (*42*), were grown in Sistrom's medium at 30 °C with 50 μg/mL spectinomycin and 2 μg/mL tetracycline. The cultures were harvested at 120 Klett units and stored at −70 °C. Frozen cells (75 g) were resuspended in 200 mL of 50 mM Tris-HCl buffer, pH 8.0, 0.5 mM EDTA, 1 mM benzamidine, 1 mM PMSF, 2 μg/mL leupeptin, and 50 μg/mL DNaseI. The cells were passed two times through a French pressure cell at 16 000 psi. Unbroken cells were removed by centrifugation at 12000*g* for 15 min at 4 °C. The supernatant was collected and centrifuged at 12500*g* for 3 h at 4 °C to pellet the membranes. The membranes were homogenized in 10 mM Tris buffer, pH 8.5, solubilized in 1.5% sucrose monolaurate (D-fructopyranosyl-D-glucopyranoside monododecanoate) and stirred at 4 °C for 30 min. Ni-NTA resin from Qiagen was allowed to bind cytochrome oxidase in the presence of 15 mM imidazole. The column was washed with 500 mL of 100 mM KH_2PO_4, pH 8.0, 0.1% sucrose monolaurate, and 30 mM imidazole. The protein was eluted with 100 mM KH_2PO_4 pH 8.0, 0.1% sucrose monolaurate, and 150 mM imidazole. The purified protein was dialyzed into 20 mM Tricine buffer, pH 8.5, containing 0.1% sucrose monolaurate and frozen with liquid nitrogen in the buffer containing 5% glycerol.

Kinetic Measurements. Rapid kinetics measurements of absorption changes were made with the Biosequential SX-17MV stopped-flow reaction analyzer from Applied Photophysics. The diode array mode (350−800 nm scan range) was used to collect spectra in the desired time window following the mixing or, alternatively, the reaction was followed at a selected wavelength using a photomultiplier. In most of the experiments shown using the photodiode array, there were 400 evenly spaced scans per data acquisition period of 78 s with 3 ms integration time for each spectrum. Before reacting with hydrogen peroxide, COX was preincubated with 200 μM ferricyanide in the presence of 10 μg/mL polylysine for 30 min to ensure full oxidation of the sample.

The reaction of COX with peroxide at acidic pH was studied using a two sequential mixing configuration of the instrument (three syringes of 1:1:1 volume ratio) so that the enzyme was mixed with the acidic buffer just 5 or 10 s before the second mixing with hydrogen peroxide. This mode of experiment allows one to avoid interference of the COX transition to the so-called "slow" form, known to occur slowly (minutes) below pH 7. The double mixing acidic pH-jump experiments were carried out as follows. In the first mixing, COX, slightly buffered at pH 8.5 (10 mM tricine), was allowed to react with hydrogen peroxide. At the time corresponding to the maximal yield of the 607 nm species, the enzyme was mixed with an 1:1 volume of 150 mM BTP buffer at pH 6.3. The final pH of the mixture was 6.5. The absorption changes following the second mixing (with the acidic buffer) were monitored. In the control experiments, the same procedure was repeated with the pH 8.5 buffer in the third syringe.

Data Analysis. Time-resolved spectra were analyzed using the Pro-K Glint Analysis software package from Applied Photophysics. First, the three-dimensional wavelength−absorbance−time data sets were reduced using singular value decomposition (SVD) to the eight most significant components (*43*). The SVD-filtered data surfaces were then subjected to a global fitting routine (*44*) according to a reaction model chosen. When necessary, the data were exported into Origin 4.0 (Microcal) and analyzed with the tools available in this software package.

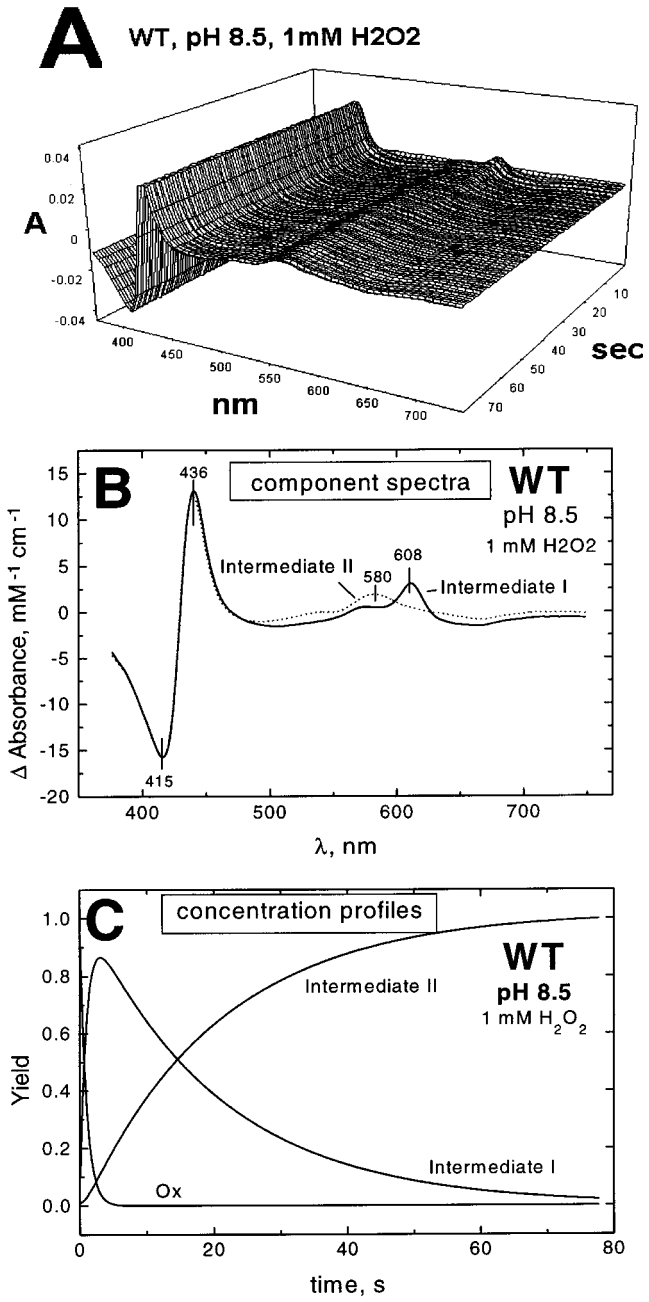

FIGURE 2: A typical set of data obtained in the stopped-flow apparatus (diode array mode) showing the reaction of 1 mM hydrogen peroxide at pH 8.5 with the oxidized cytochrome *c* oxidase from *R. sphaeroides*. Four hundred scans were collected during an observation period of 77 s. (A) The SVD-reduced spectra set. (B) Difference spectra of the two intermediates resolved by the global fitting routine. (C) Time-evolution of the two intermediates.

RESULTS

Reaction of WT COX with Hydrogen Peroxide at pH 8.5. Figure 2 shows a typical set of results obtained upon rapid mixing of wild-type COX with 1 mM hydrogen peroxide at pH 8.5. Panel A presents the experimental data, panel B gives the difference spectra (referenced to the oxidized state) of the two intermediates resolved by global fitting of the SVD-filtered data, and panel C shows the time evolution of the intermediates. Global analysis of the spectroscopic changes following the mixing of the *R. sphaeroides* COX with different concentrations of H_2O_2 at pH 8.5 consistently

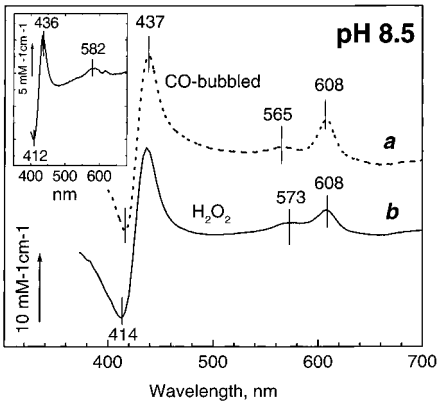

FIGURE 3: Difference spectra of the pure $\mathbf{P}_{607}$ state generated by aerobic CO-bubbling (a) and of the peroxide-induced intermediate I (b). Main panel: the spectra have been normalized by their Soret band response. Inset: the two spectra have been normalized by the height of the band at 608 nm (vs 630 nm reference), and the difference (H_2O_2-treated minus CO-bubbled) is shown in the panel.

resolves the sequential formation of two intermediates: **Ox** → intermediate I → intermediate II (→ **Ox**).

At 1 mM H_2O_2, intermediate I rises and decays to intermediate II with rate constants of ca. 1 and 0.05 s^{-1} (Figure 2C). The last step (intermediate II → **Ox**) can be included optionally in the model in accordance with the cyclic reaction sequence proposed in ref *22*, but global analysis invariably finds this step slow as compared to the preceding two steps, and its inclusion does not affect the rate constants k_1 and k_2 found for the **Ox** → intermediate I and intermediate I → intermediate II transitions, respectively. This is consistent with the conclusion of Junemann et al. (*28*) from studies of the bovine oxidase and agrees with the earlier reports that the peroxide-dependent regeneration of the **Ox** state from compound **F** is the rate-limiting step of the peroxide cycle with bovine COX [2−4 M^{-1} s^{-1} at pH 7 (*24*)].

Intermediates I and II have very similar (although not identical) Soret bands but differ significantly in the visible region of the spectrum (Figure 2B). The difference spectrum of intermediate II, with a maximum at ca. 580 nm, is typical of the conventional ferryl-oxo state or "compound **F**". The spectrum of intermediate I is dominated in the visible by a peak at 607−608 nm, diagnostic of the so-called "peroxy" state. Analogous results were obtained earlier with bovine COX (*28*, *45*, *46*) and have been often interpreted as sequential generation of the "peroxy" (607 nm) and ferryl-oxo (∼580 nm) states in a consecutive reaction of COX with two molecules of H_2O_2 as initially proposed in ref *22* (Scheme 1). However, the situation is more complicated, since the absorption characteristics of intermediate I in the visible are not identical to those of pure compound $\mathbf{P}_{607}$. For example, the apparent extinction coefficient of intermediate I at 607 nm is around 5−6 mM^{-1} cm^{-1}, whereas that for the pure compound $\mathbf{P}_{607}$ is 10−12 mM^{-1} cm^{-1} (*47*, *48*). The differences between intermediate I and pure compound $\mathbf{P}_{607}$ become obvious from the analysis of the line shapes of their difference spectra.

In the difference spectrum of the pure Peroxy state, generated by the aerobic CO bubbling method (*49*), the β-band has a peak at ca. 565 nm, the $\Delta A608/\Delta A565$ ratio is around 4, and the $\Delta A\text{Soret}_{max-min}/\Delta A_{607-630}$ is 4.8 (Figure 3,

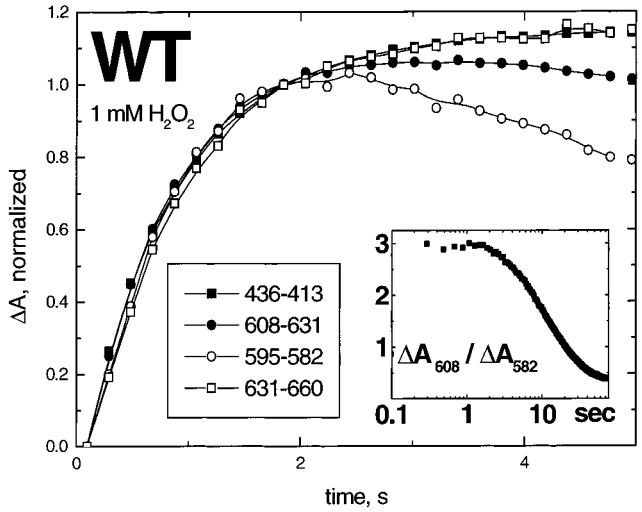

FIGURE 4: Simultaneous rise of the 607 and 580 nm states during the initial phase of H_2O_2 reaction with COX. Main panel: Absorption changes at the indicated wavelength pairs have been extracted from the data set shown in Figure 2A and normalized by their magnitude at 1.85 s. The first scan (~0.2 s; reaction progress, ca. 10%) has been subtracted as a baseline from all subsequent scans for construction of the difference spectra series. Inset: The ratio of Δ*A* at 608 and 582 nm in the difference spectra induced by peroxide binding is maintained constant during the initial reaction phase (ca. 2 s) corresponding to rise of intermediate I. Note that a log time scale is used in the inset.

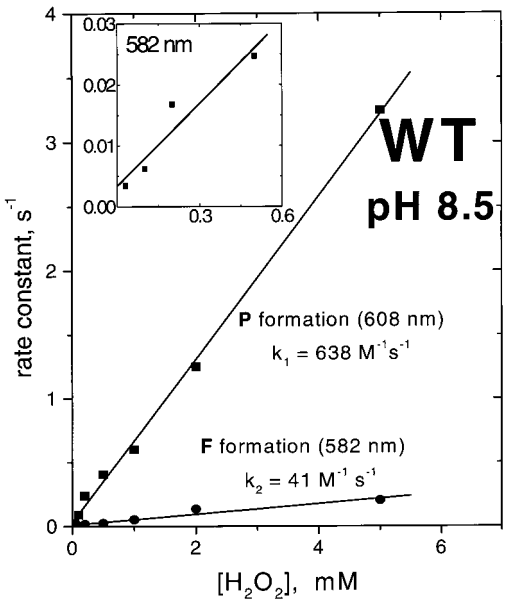

FIGURE 5: H_2O_2 concentration-dependence of the rates of formation of intermediates I and II during the reaction of COX with hydrogen peroxide. Stopped-flow experiments were carried out at pH 8.5 at different concentrations of hydrogen peroxide and the reaction kinetics were monitored at several selected wavelengths to follow formation of intermediate I (**P** in the figure) and its subsequent conversion to intermediate II (**F** in the figure). Absorbance changes at both 608 and 582 nm are biphasic. In the figure, the apparent first-order rate constants have been plotted for the first phase of absorbance changes at 608 nm (rise phase), and the major (second) phase of absorbance increase at 582 nm. The pseudo first-order rate constants for the rise of A_{608} agreed well with those obtained from the measurements at 436 nm (not shown). Inset: experiments at low peroxide concentrations indicate an extrapolated nonzero rate of formation of intermediate II (0.0030 ± 0.0019 s^{-1}).

curve a), in excellent agreement with the data reported for bovine COX (*27*, *48*). At the same time, the *β*-band of intermediate I is located at 571−572 nm and the Δ*A*608/Δ*A*571 ratio (measured vs the 630 nm reference point) is ~2.7 while the *γ*/α ratio is 7.8 (Figure 2B). Such a line shape is diagnostic of a mixture of the $\mathbf{P}_{607}$ and $\mathbf{F}_{580}$ states. This is illustrated clearly by Figure 3, which compares the spectrum of compound $\mathbf{P}_{607}$, generated by aerobic CO-bubbling, and the absorption changes induced by the reaction with 1 mM H_2O_2 3.6 s after mixing, which corresponds to the maximal yield of intermediate I (~90%, Figure 2C). By normalizing these two spectra by their Soret bands (main panel), the 607 nm band of the peroxide-induced species (vs the 630 nm reference point) corresponds to only a 62% yield of the compound **P**. Subtracting this component from the spectrum of intermediate I gives a spectrum typical of a ferryl-oxo state, shown in the inset of Figure 3. Thus, it is clear, that intermediate I is spectroscopically heterogeneous and represents a mixture of the peroxy and ferryl-oxo states in a ca. 2:1 ratio. Similar results confirming the spectral heterogeneity of intermediate I have been obtained at peroxide concentrations up to 20 mM.

Despite spectral heterogeneity, intermediate I is generated as a single species. Absorption changes at different characteristic wavelengths specific for formation of intermediates $\mathbf{P}_{607}$, $\mathbf{F}_{580}$ and for the decay of the free oxidized state develop simultaneously (Figure 4), and the line shapes of the difference spectra recorded during the rise phase of intermediate I are identical within experimental scatter. This can be illustrated by the time dependence of the ratio Δ*A*608/Δ*A*582 (Figure 4, inset) which is very sensitive to the fractional contributions of the 607 and 580 states. The ratio of ~3 remains constant throughout the rise of intermediate I (ca. 2s), and then decreases to zero as intermediate I converts to intermediate II.

At peroxide concentrations below 0.5 mM, the second phase of the reaction (607 → 580 transition) is incomplete. At progressively lower concentrations of peroxide, the spectrum of intermediate II, as found by global fitting, approaches that of intermediate I. Apparently, at low peroxide concentrations, the reaction monophasically approaches a steady-state mixture of the 607 and 580 states as observed previously in hand-mixing experiments (*25*, *28*).

The rate of the reaction of COX with peroxide was been studied using a range of concentrations of H_2O_2 from 0.1 to 20 mM. In addition to the analysis by global fitting of the spectra, a series of experiments were carried out by directly monitoring the kinetics of the absorption changes at selected wavelengths (608, 582, and 436 nm). The rates of both the initial reaction of peroxide with the enzyme (**Ox** → intermediate I, monitored by an increase in A_{436} or A_{608}) and decay of intermediate I to intermediate II (monitored by a decrease of the absorbance at 608 nm or by an increase of the absorbance at 582 nm, with no significant difference between the results) are linearly proportional to peroxide concentration (Figure 5). The second-order rate constants are around 10^3 M^{-1} s^{-1} for k_1 (600−1000 M^{-1} s^{-1}) and 40−60 mM^{-1} s^{-1} for k_2 depending on preparation and method of data analysis (e.g., the rate constants found by global fitting analysis may differ slightly from those determined by exponential fitting of the kinetic curves at 608 minus 631 nm or 436 minus 413 nm extracted from the same data set). These values are in reasonable agreement with the earlier data on bovine COX (*28*, *45*, *46*) but are about 4-fold higher than the rate constants

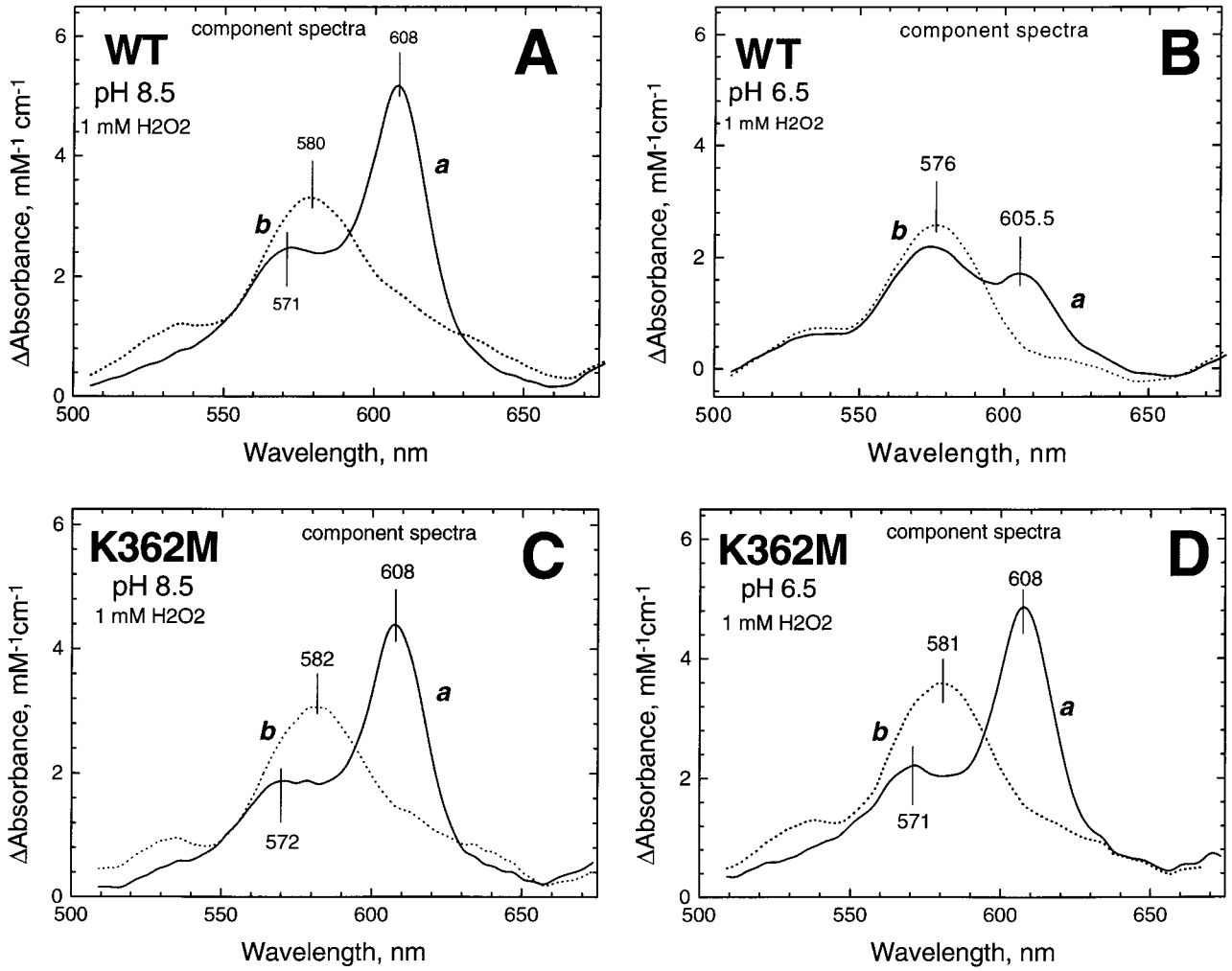

FIGURE 6: Reactions of 1 mM hydrogen peroxide with the WT oxidase (A, B) and the K362M mutant (C, D) at alkaline and acidic pH. The reaction has been monitored in a stopped-flow apparatus (diode array mode) as in Figure 2. Experiments at pH 6.5 have been performed in a double mixing configuration of the instrument. COX, weakly buffered at pH 8.5, has been mixed with the strong acidic buffer (150 mM BTP, pH 6.3, final pH 6.5) 5 s before the second mixing with hydrogen peroxide (1 mM final concentration). The panels show the difference spectra of the two intermediates in the α-band resolved by global fitting.

previously reported for *R. sphaeroides* COX (0.6 and 0.05 s^{-1} at 4 mM H_2O_2 and pH 8; ref *51*). It is noteworthy that the plot of the rate of formation of intermediate II versus $[H_2O_2]$ crosses the ordinate axis slightly above the origin, at about 0.003 s^{-1}, extrapolating at zero peroxide concentrations (Figure 5, inset). This indicates the possibility of a slow peroxide-independent decay of intermediate I (cf. ref *27*), presumably due to adventitious reductants in the buffers or intraprotein sources of reducing equivalents.

Comparison of the Peroxide Reaction with the WT and K362M Oxidases at pH 8.5. Behaviors of the WT and K362M COX are compared in Figures 6 and 7. Only the visible portion of the spectra are displayed, since this emphasizes the region where the intermediates are most clearly distinguished spectroscopically. The Soret regions of the spectra differ only slightly for the two intermediates. At pH 8.5, the pattern of the reaction of hydrogen peroxide with the mutant K362M COX is similar to that of the wild-type enzyme (Figure 6 A,C; Figure 7A). The differences in the peroxide interactions of K362M and WT COX as reported by Mills and Ferguson-Miller (*52*) were not observed. In each case, the initial difference spectrum shows formation of a species with an α-peak at 608 nm which transforms to a compound with an α-peak around 580 nm. The rate constants for generation and decay of intermediate I and its subsequent conversion to intermediate II are similar in WT and K362M mutant (Figure 7A, Table 1), as are the spectral characteristics of the intermediates (Figure 6A,C).

Comparison of the Peroxide Reaction with the WT and K362M Oxidases at pH 6.5. In contrast to the similarities observed for the WT and mutant enzymes at pH 8.5, the reaction with hydrogen peroxide at pH 6.5 reveals striking differences between K362M and WT. In the wild type COX, much less of the 607 nm species is formed at pH 6.5 as compared to pH 8.5, and the initial product observed is largely a 580 nm-type state with an absorption peak near 575 nm. Global fitting of the absorbance changes in the α-band still reveals two components (Figure 6B), but the species that is responsible for the 607 nm peak in the spectrum of the first component is much less than at pH 8.5 and reveals a markedly blue-shifted maximum at 605−606 nm. In addition, the difference spectrum of intermediate II formed at acidic pH shows a peak at about 576 nm rather than at 580 nm (Figure 6B). Such a blue-shifted peak position of the peroxide product of COX at acidic pH was noticed previously for the bovine oxidase ((*25*−*27*, *53*), Vygodina,

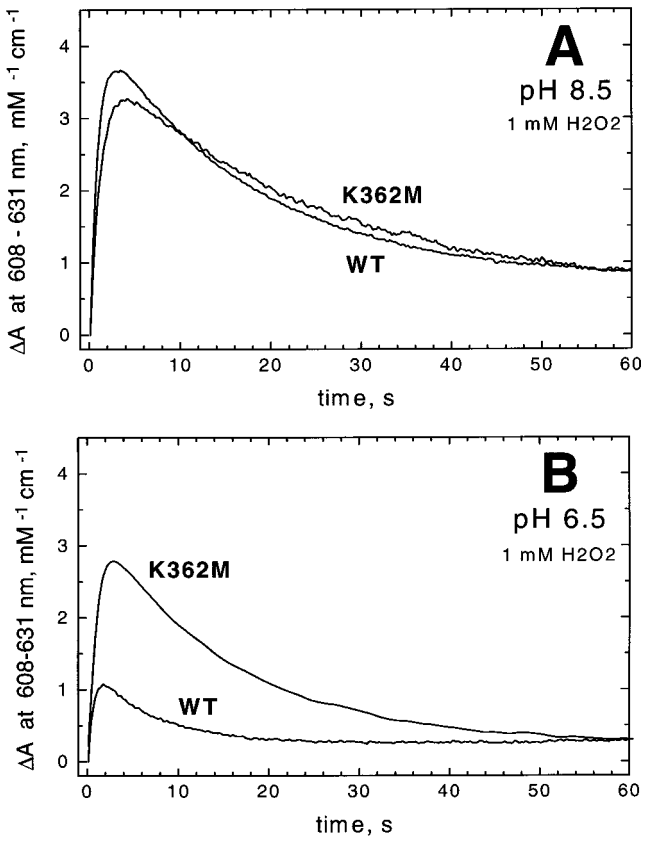

FIGURE 7: Kinetics of the appearance and decay of the 607 nm species for the WT and K362M mutants in the reaction with 1 mM peroxide at pH 8.5 (A) and at pH 6.5 (B). The kinetic traces have been extracted from the same time/spectra surfaces as used for resolution of component spectra in Figure 6.

Table 1: Apparent First-Order Rate Constants for Rise (k_1) and Decay (k_2) of Intermediate I upon Reaction of COX with 1 mM H_2O_2 at pH 8.5 and pH 6.5 for the WT, K362M, and D132N *R. Sphaeroides* Oxidase

	WT, pH 8.5	WT, pH 6.5	K362M, pH 8.5	K362M, pH 6.5	D132N, pH 8.5	D132N, pH6.5
k_1 (s^{-1})	0.99	1.2	0.81	0.90	0.88	1.03
k_2 (s^{-1})	0.050	0.17	0.042	0.089	0.043	0.050

Ponamarev, Konstantinov, in preparation). The rise time for the first component at pH 6.5 is essentially the same as at pH 8.5 (k_1 values of 1.17 and 0.99 s^{-1}, respectively); however, the disappearance of the ~607 nm peak is markedly faster at pH 6.5 (0.17 vs 0.05 s^{-1}) (Table 1).

In contrast, the reaction of peroxide with the K362M COX at pH 6.5 remains essentially the same as at alkaline pH, with clear initial formation of the peak at 608 nm. Global fitting resolves the same two components at pH 6.5 as observed at pH 8.5 (Figure 6C,D). Notably, the 607 nm species forms at pH 6.5 to the same extent and with the same peak position as at pH 8.5. However, the second intermediate formed at pH 6.5 with the K362M mutant has an absorption maximum at 581−582 nm, rather than at 575−576 nm as in WT enzyme (cf. panels B and D in Figure 6). The rate of formation of the first intermediate in the reaction of peroxide with K362M at pH 6.5 is essentially the same as at pH 8.5. The rate of decay of the 607 nm peak and the concomitant formation of the second intermediate is, however, 2-fold faster than at pH 8.5 (Table 1). The kinetics of the formation and decay of the species absorbing at 608 nm with the WT and K362M oxidases are compared directly in Figure 7. Whereas at pH 8.5 the kinetic traces ($\Delta A_{608-631}$) for the WT and K362M oxidases are fairly close to each other (Figure 7A), at pH 6.5 the yield of the 607 nm species is much greater in K362M as compared to the WT oxidase (Figure 7B).

Conversion from the 607 nm to the 580 nm Species Induced by an Acidic pH Jump. Once the 607 nm peroxide product has formed at pH 8.5, acidification brings about its decay to the 580 nm species. This effect is observed in the WT enzyme as well as in the proton-channel mutants K362M and D132N and is rather slow at low peroxide concentrations. A similar slow rate of the 607 nm → 580 nm conversion in response to the acid pH-jump has been noticed also with bovine COX ((*28*), Vygodina, Konstantinov, unpublished).

The acid pH-jump experiments were carried out in a two sequential mixing configuration of the instrument as described in Materials and Methods over a 100-fold range of H_2O_2 concentrations (0.05−10 mM after the second mixing). Global analysis of the data show that the acidic pH-jump promotes decay of the 607 nm intermediate to a 580-type state with both the WT and K362M COX, and at all H_2O_2 concentrations. The decay could be fitted reasonably well assuming a single step a → b model. At peroxide concentrations above 1 mM, the conversion is dominated by the conventional peroxide-dependent intermediate I → intermediate II reaction that also takes place at pH 8.5, as described above (cf. Figure 2). Notably, this reaction is accelerated by acidic pH in the WT COX more significantly than in K362M COX (e.g., Table 1), the difference increasing at higher peroxide concentrations. For instance, decay of the 607 state observed after acidic pH-jump in the presence of 2.5 mM H_2O_2 is about 3−4-fold faster in wild-type COX than in K362M (data not shown).

To elicit the peroxide-independent, pH-induced transition it is necessary to carry out the reaction at H_2O_2 concentrations below ~200 μM. Under these conditions, the acidic pH-jump induces rather slow decay ($\tau \sim 40$ s in wild-type enzyme) of the 607 state to a 580-type intermediate. A typical series of spectral scans observed in the course of such an experiment with wild-type COX is shown in Figure 8A. Essentially, the same 607 → 580 transition is observed with the K362M and D132N mutants (Figure 8B) and, hence, neither the K- nor D-channel is likely to be specifically involved in this transition. The fact that the conversion does occur in K362M shows that the $\mathbf{P}_{607}$ state of the mutant does "sense" the acidic pH. Hence, the insensitivity of the K362M mutant to acidic pH in the H_2O_2-binding experiments (Figures 6 and 7) is not likely to be due to a simple p*K* shift of a residue in the enzyme. Rather, the K362M mutation inhibits proton delivery to the active site through the K-channel in those experiments.

Incubation of the K362M Mutant at pH 6.5 Prior to the Reaction with Peroxide Does Not Affect the Reaction. In the experiments in which the reaction of either the WT or mutant oxidase was examined at pH 6.5 (Figure 6), the enzyme was usually exposed to the mildly acidic conditions for 5 s prior to the addition of peroxide (see Materials and Methods). This double mixing technique was employed to avoid artifacts arising from formation of the "slow" enzyme species which will occur upon prolonged exposure to acidic conditions. It

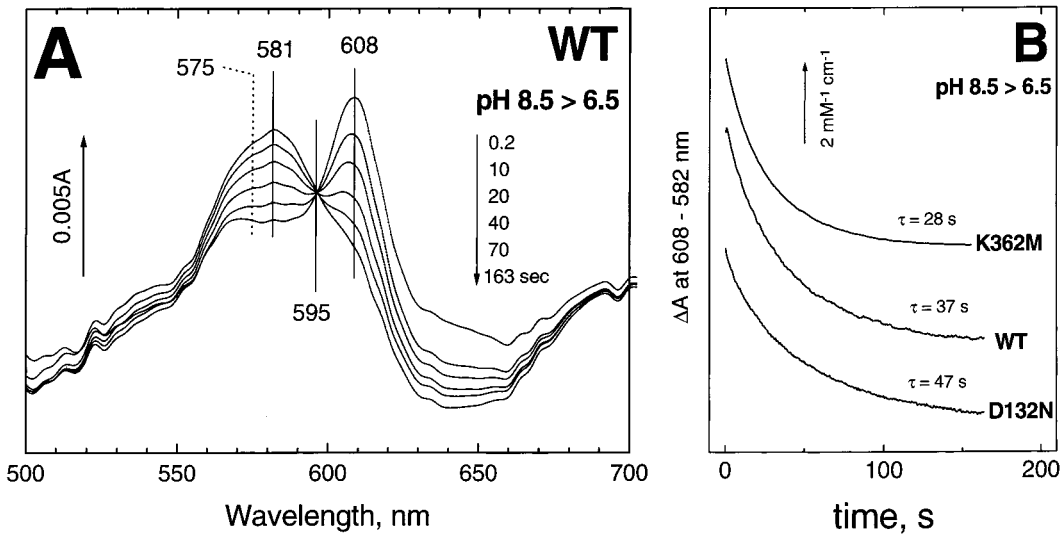

FIGURE 8: Decay of the $\mathbf{P}_{607}$ state induced by acid pH-jump in WT and mutant COX. Experiments have been performed in a double mixing configuration of the stopped-flow apparatus (see Materials and Methods). Weakly buffered COX at pH 8.5 has been mixed first with H_2O_2 (100 μM after mixing), and 1 min incubation was allowed for the 607 nm intermediate to reach steady-state level. Subsequently, the pH was shifted to 6.5 by a second mixing with the acidic pH buffer. The spectra obtained in the control mixing experiments without H_2O_2 have been used as a baseline for construction of the difference spectra. See the text for other details. (A) Representative difference spectra observed with wild-type COX. (B) Kinetics of the 607 → 580 transition induced by an acid pH-jump in wild type, K362M, and D132N COX. The curves have been extracted from the time/spectra surfaces.

is conceivable that exposure of the K362M mutant to acidic pH for a longer period could overcome the kinetic block to proton uptake that is imposed by the mutation and, thereby, restore the "wild type" behavior to the K362M mutant at pH 6.5. This possibility was examined. Experiments were carried out in which the oxidized K362M COX was preincubated with acidic buffer (pH 6.5) for 1, 5, 10, 20, 60, 180, or 300 s before the second mixing with H_2O_2 (1 mM final concentration). Surprisingly, it was observed that exposure of the oxidized K362M COX to acidic pH *prior* to mixing with peroxide does not significantly affect the reaction. The yield of the 607 state is essentially the same in the experiments with 1 s or 5 min preincubation at pH 6.5 (Figure 9). Note that when the acidic pH-jump is made *following* the formation of the 607 nm state at pH 8.5, about 2 min is sufficient for complete H^+-induced decay of the $\mathbf{P}_{607}$ state of the K362M mutant, as described in the previous section (Figure 8). Taken together, these observations may indicate that the binding of peroxide to the enzyme must precede or be simultaneous with the protonation event that is blocked by the K362M mutation. Hence, longer exposure to acid pH prior to the addition of peroxide has no influence on the subsequent reaction kinetics.

Reaction of Peroxide with the D132N Mutant Oxidase. To a first approximation, the reaction of the D132N mutant COX with H_2O_2 is the same as the WT oxidase, both at pH 8.5 and at pH 6.5 (Figure 10). At pH 8.5, the 607 nm species rises and decays with rate constants similar to those in WT or K362M (Figure 10C, Table 1). At pH 6.5, the yield of the 607 nm species formed with the D132N mutant greatly diminishes, and the absorption peak shifts to ~606 nm (Figure 10B), which is also observed with the WT COX (Figure 6B). A somewhat higher apparent yield of the "607 nm" species at pH 6.5, and incomplete return of the $\Delta A_{608-631}$ traces to the zero level during the intermediate I → intermediate II transition were often observed in the peroxide reaction with the D132N mutant. This is at least partially

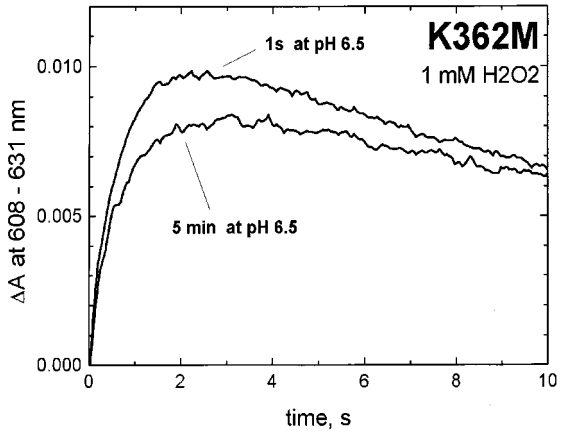

FIGURE 9: Effect of preincubation of the K362M mutant at acidic pH on the yield of the 607 state. K362M oxidase (16.8 μM) in 10 mM tricine buffer, pH 8.5, was preincubated for 30 min with 0.2 mM ferricyanide and 10 μg/mL of polylysine for complete oxidation. The enzyme was then mixed sequentially, first with an equal volume of 150 mM BTP-buffer, pH 6.3 (final pH 6.5), and, after incubation at pH 6.5 for the indicated time period, mixed with an equal volume of 2 mM peroxide in 75 mM BTP at pH 6.5. Final concentrations: 4.2 μM COX, 1 mM peroxide, 75 mM BTP buffer, pH 6.5. Absorption changes following the second mixing were monitored in a diode array mode (ca. 20 s/400 scans). The first scan (after 28 ms, less than 10% of the overall spectral change) was taken as a baseline for construction of the difference spectra showing subsequent spectral changes. The kinetics traces shown have been extracted from the corresponding spectra/time surfaces.

due to slow formation in the D132N mutant of alternative states absorbing near 600 nm. These secondary processes varied for different preparations and will require separate investigation. It is noteworthy that with the WT and, to a lesser extent, with the K362M COX, the peroxide-induced decay of the 607 species to intermediate II is accelerated at acidic pH, but that this is not the case with the D132N mutant. This suggests that the D-channel is involved in the transitions following the formation of intermediate I in the reaction with peroxide.

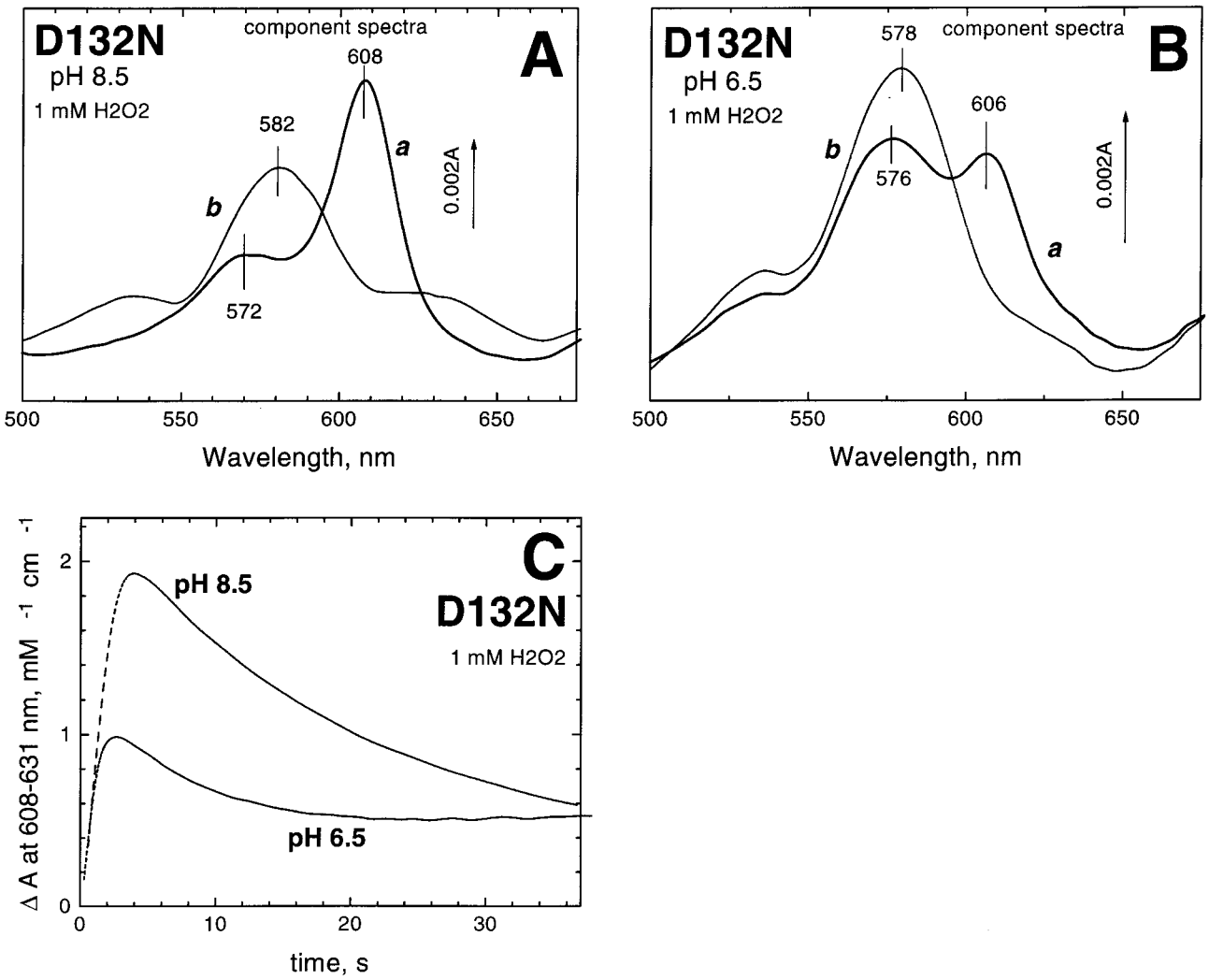

FIGURE 10: Reaction of 1 mM hydrogen peroxide with the D132N mutant at pH 8.5 and pH 6.5. The reaction was carried out as in the case of wild type of K362M oxidases. (A, B) Difference spectra of the two intermediates resolved by global fitting of the absorption changes at pH 8.5 and pH 6.5. (C) Kinetics of the absorption changes at 608 nm observed at alkaline and acidic pH.

DISCUSSION

There have been several previous time-resolved studies of the reaction of hydrogen peroxide with oxidized COX, all of them performed with the bovine COX (*45*, *46*, *54*−*56*). The current work is the first detailed investigation in which the peroxide reaction with a bacterial cytochrome *c* oxidase has been monitored on a time-resolved basis in the entire UV/vis range, as done earlier with the bo_3-type quinol-oxidase from *E. coli* (*29*). It is worthwhile to first compare the basic results obtained in this work with COX from *R. sphaeroides* to what is known from the previous experiments with the bovine oxidase.

Reaction at Alkaline pH. Interaction of the oxidized *R. sphaeroides* COX with H_2O_2 shows essentially the same pattern as does the reaction of bovine COX. As mentioned above, pre-steady-state kinetics of the reaction at pH 8.5 can be described by sequential formation of two intermediates: **Ox** → intermediate I → intermediate II, where intermediate II has spectral characteristics of the conventional compound **F** (580 nm species), while intermediate I is dominated in the visible by contribution of the so-called "Peroxy" state ($\mathbf{P}_{607}$ species). Analogous observations were made earlier in the time-resolved studies at selected wavelengths with bovine COX (*46*) and are often interpreted as serial formation of compounds $\mathbf{P}_{607}$ and $\mathbf{F}_{580}$ (Scheme 1). However, the current data show that intermediate I at pH 8.5, while resolved as a single species kinetically, is spectroscopically heterogeneous and is a mixture of $\mathbf{P}_{607}$- and $\mathbf{F}_{580}$-type states (Figures 2−4). This is consistent with earlier conclusions that the 607 nm species of the bovine COX, observed under steady-state conditions at low peroxide concentrations, is not a pure $\mathbf{P}_{607}$ state but, rather, a mixture of $\mathbf{P}_{607}$ and $\mathbf{F}_{580}$ species (*26*, *27*). Since the $\mathbf{F}_{580}$-type species are found both as part of intermediate I and as intermediate II, they are denoted as two separate species, $\mathbf{F\text{-}I}_{580}$ and $\mathbf{F\text{-}II}_{580}$, in a modified reaction scheme (Scheme 2). Species $\mathbf{F\text{-}I}_{580}$ is presumed to be at a redox state two-electrons removed from the fully oxidized enzyme, whereas $\mathbf{F\text{-}II}_{580}$ is only one electron from **Ox**.

Scheme 2

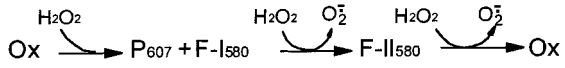

Intermediate I

Reaction at Acidic pH. The reaction of bovine COX with H_2O_2 at acidic pH has been long known to proceed differently

from the reaction at pH 8.5. In 1987, Vygodina and Konstantinov reported (*53*) that the peroxy complex of liposome-reconstituted bovine COX formed at pH 6, with H_2O_2 concentrations as low as 0.3−0.5 μM (stoichiometric with COX under the experimental conditions), exhibits normal Soret band characteristics but lacks the 607 nm band. Thus, the intermediate spectroscopically resembles the alkaline compound **F**, but with the α-peak closer to 570 nm rather than at 580 nm. It was proposed that, while the changes in the Soret band and in the peak at 570−580 nm are induced by the interaction of H_2O_2 with heme a_3, the 607 nm band may report a special high-energy deprotonated state of COX stabilized by H_2O_2-induced changes at Cu_B, the relaxation of which can be coupled to electrogenic proton uptake from the matrix phase (*25*, *53*). A similar idea of the energy-coupled decay of the 607 nm state has been considered in a recent model of Michel (*30*). The experimental finding of the absence of the 607 nm species resulting from the peroxide reaction at acid pH was confirmed by Fabian and Palmer (*27*) with solubilized COX. These authors assumed, in contrast to ref *53*, that the species without the 607 nm band generated by low-peroxide concentrations at acidic pH is identical to the alkaline compound **F**, which led them to postulate an inverse order of formation of the intermediates, with a linear sequence: **Ox** → $\mathbf{F}_{580}$ → $\mathbf{P}_{607}$ (*27*). However, as all the above experiments were carried out on a time scale of minutes, transient generation and decay of the 607 nm state at acidic pH was difficult to exclude.

The current time-resolved experiments with the *R. sphaeroides* oxidase show, indeed, that transient generation of a 607 species can be resolved at pH as low as 6.5, but its yield is much lower than at pH 8.5. Importantly, increasing the H_2O_2 concentration in the range 0.5−10 mM does not significantly affect the yield of the 607 nm species at pH 6.5. Thus, at acidic pH, the major initial product of the reaction with peroxide is a 580-type intermediate that lacks the 607 nm band. The form of intermediate I that is observed at acid pH is denoted as species $\mathbf{F\text{-}I}_{575}$. The spectrum of this species has a distinctly blue-shifted α-band (Figure 6B), in agreement with the earlier data on bovine COX, where the acidic low-peroxide product of COX was reported to absorb closer to 570 nm rather than at 580 nm (*25*, *26*, *53*) (cf. also ref *27*). The $\mathbf{F\text{-}I}_{575}$ species is probably equivalent to the $\mathbf{F}^{\bullet}$ (*28*) or **F′** (*29*, *30*) states, which have been described for the bovine oxidase and the cytochrome bo_3 quinol oxidase.

Reaction Branching. The simultaneous rise of the 607 nm- and 580 nm-type compounds in the first phase of the COX reaction with H_2O_2 supports an idea of the reaction branching (*28*, *29*). Two simple schemes can be considered (cf. *28*): (A) the reaction branches at a level of intermediate I, i.e., $\mathbf{P}_{607}$ is in rapid equilibrium with an isoelectronic species that is spectroscopically similar to compound $\mathbf{F}_{580}$ (Scheme 3A) or (B) the reaction branches prior to intermediate I (Scheme 3B).

A particular version of model **3A** has been considered previously (*28*, *29*), in which the $\mathbf{P}_{607}$ nm state is formed initially upon peroxide binding and converts rapidly to **F′** ($\mathbf{F}^{\bullet}$, $\mathbf{F\text{-}I}_{575}$) in a H^+-dependent reaction. However, if equilibration between the two intermediate I species is much faster than peroxide binding, one actually cannot say which of the two states within the intermediate I box is formed first.

Scheme 3

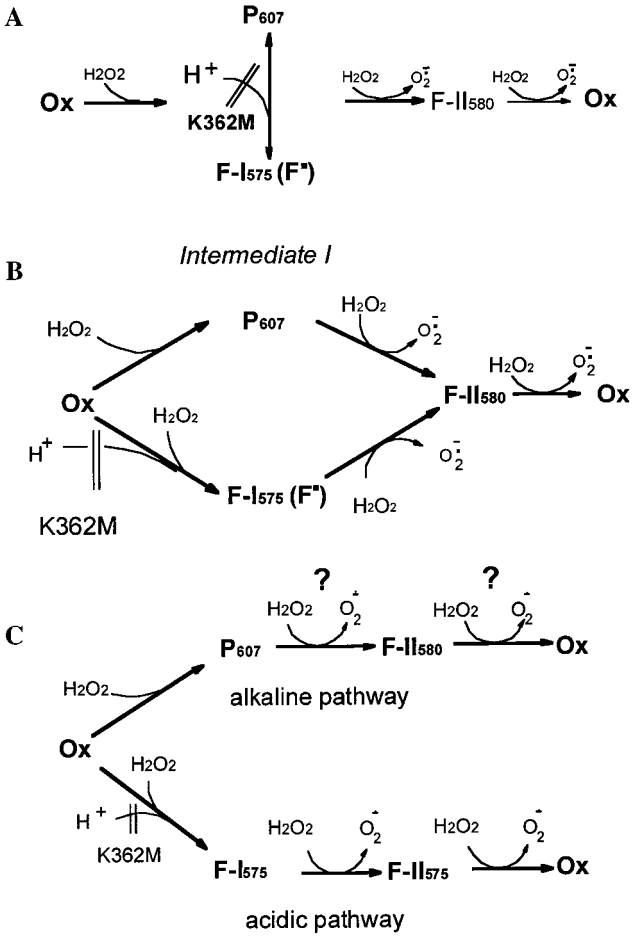

The effect of an acid pH-jump on the rate of conversion of $\mathbf{P}_{607}$ to an $\mathbf{F}_{580}$ state could allow one to discriminate between models **3A** and **3B** (*28*). This effect was examined in the WT, K362M, and D132N COX (Figure 8). Once the $\mathbf{P}_{607}$ state is formed in a reaction of COX with H_2O_2 at pH 8.5, the acid jump induces a decay of the $\mathbf{P}_{607}$ state to a 580-type intermediate that is, however, quite slow (τ ca. 30−50 s) and is not influenced significantly by the K362M or D132N mutation. This finding may suggest that $\mathbf{P}_{607}$ is not in rapid intramolecular equilibrium with $\mathbf{F\text{-}I}_{575}$, as assumed by Scheme 3A, but rather that the two species are formed in different populations of COX and are not directly interconvertible, as shown in Scheme 3B. An analogous argument in favor of the reaction branching at the level of the **Ox** state in bovine cytochrome *c* oxidase (rather than at the level of the **P** intermediate, as proposed originally by Brittain et al. for the cytochrome bo_3 quinol oxidase (*29*)) has been put forward in recent work of Junemann et al. (*28*). However, this interpretation, although plausible, relies tacitly on the assumption that the protonatable group(s) affecting the 607 → 580 balance in intermediate I is freely accessible to protons from the bulk phase. As discussed below this is not necessarily the case.

There are several qualitative questions raised by the reaction branching model in Scheme 3B.

(1) Is there a common compound $\mathbf{F\text{-}II}_{580}$ state for the alkaline and acidic pathways? In Scheme 3B, the acid and alkaline reaction pathways merge at the level of compound **F-II**. Both $\mathbf{P}_{607}$ and $\mathbf{F\text{-}I}_{575}$ ($\mathbf{F}^{\bullet}$), in this scheme, react with a

second molecule of peroxide, yielding superoxide and converting to the same **F-II**$_{580}$ state (e.g., refs *28* and *30*). In view of the spectral similarity between the multiple 580-type states, it is not easy to verify such a proposal by direct experimental observations. An obvious alternative is that the acid and alkaline pathways do not merge at the level of **F-II**$_{580}$, but, rather, there are two fully independent reaction routes for the protonated and unprotonated enzyme (Scheme 3C).

The finding that the difference spectrum of the peroxide-induced changes at pH 6.5 shows a maximum at 575−576 nm for both intermediates I and II, rather than at 580−585 nm, as typical of the alkaline compound **F** (*22*, *51*, *57*−*59*), may favor Scheme 3C.

(2) Does the enzyme cycle at all via the alkaline pathway? The reaction of H_2O_2 with COX is accompanied by superoxide generation (*23*, *24*) which is assigned traditionally to sequential single-electron reduction of compound **P**$_{607}$ to compound **F**$_{580}$ and of compound **F**$_{580}$ back to the **Ox** state (*22*, *24*, *28*, *30*) (Schemes 1−3). Notably, the rate of superoxide generation decreases almost to zero with alkalinization from pH 6 to pH 9 ((*23*), Vygodina, Peskin, and Konstantinov, unpublished) which parallels the pH-dependence of the contribution of the acidic pathway in Scheme 3B or C. It is, therefore, possible that superoxide generation is associated mainly, or even exclusively, with the contribution of the acidic pathway in Scheme 3B or C. Accordingly, the question of whether the **P**$_{607}$ → **F-II**$_{580}$ and/or **F-II**$_{580}$ → **Ox** transitions occur by the above-mentioned superoxide-generating mechanism may need reinvestigation. It is noteworthy that the analysis of Scheme 3B by Junemann et al. (*28*) predicts the **F** → **Ox** transition at pH 6 to be about 50-fold slower than at pH 8 (see Table 2 in ref *28*). In contrast, the overall pseudo-catalase cycle of COX **Ox** → intermediate I→ intermediate II → **Ox**, as followed by the rate of superoxide generation and limited by the rate of the **F** → **Ox** transition, is much faster at acidic pH (*23*, *24*). Finally, the steady-state peroxidase activity of COX increases upon acidification in the same range as the contribution of the acidic pathway (*17*) and may also be specifically associated with the oxidation of ferrocyanide by intermediates of the acidic pathway, rather than by **P**$_{607}$.

(3) Is the pH-dependent branching at the **Ox** → intermediate I step associated with proton uptake in the acidic pathway or with proton release in the alkaline pathway? These alternative assumptions are made by Junemann et al. (*28*) and Michel (*30*), respectively, while considering an otherwise similar branching mechanism. Inhibition of the *acidic* pathway by the K362M mutation is much more naturally explained by a proton uptake mechanism, and, therefore, only this variant of branching has been considered above (Scheme 3).

(4) Does proton uptake precede peroxide binding in the acidic pathway? If protonation of COX via the K-channel in the acidic pathway is independent of the reaction with H_2O_2 and precedes peroxide binding with heme a_3, one would expect that prolonged exposure of K362M to acidic pH before mixing with peroxide would restore WT behavior to the mutant by routing the reaction with H_2O_2, through the acidic pathway. However, the experimental result (Figure 9) is that exposure of the oxidized K362M COX to acidic pH prior to mixing with peroxide does not significantly affect the reaction, and that the yield of the **P**$_{607}$ state is much the same for the experiments with 1 s or 5 min preincubation times at pH 6.5. This result suggests that, in the acidic pathway, the proton is taken up by the enzyme *after* peroxide binding or simultaneously with it (e.g., if the two events are coupled). In general, peroxide binding could promote proton uptake kinetically (e.g., connecting the K-channel), thermodynamically (raising the p*K* of the group(s) involved), or by creating new proton accepting group(s) in the course of the chemical reaction that peroxide undergoes in the binuclear site. A specific mechanism for peroxide-dependent proton binding is considered in the scheme shown in Figure 11.

A less likely alternative is that in the oxidized K362M COX, protonation of the binuclear center takes very much longer than 5 min (e.g., hours). This hypothesis is difficult to test directly since incubation of COX at acidic pH for tens of minutes will result in the fast-to-slow transition of the enzyme and loss of peroxide reactivity. It is noted, however, that the reduction of heme a_3 by dithionite is limited by the delivery of a proton via the K-channel, and this process has a halftime of just a few minutes for the major fraction of the enzyme (*19*).

(5) Is 607 state the sole initial product formed in the alkaline pathway? As discussed above, the initial phase of the reaction of COX with H_2O_2 at pH 8.5 gives an intermediate I that is a mixture of the 607 and 580 nm states, rather than pure **P**$_{607}$ (see Figures 3 and 4). The simplest interpretation is that the 607 nm species is generated in the alkaline pathway while the 580 nm component is formed solely via the acidic route (*28*, *30*) (Scheme 3B,C), and that both pathways are functional at pH as high as pH 8.5. However, there are two results that do not fit this simple model. First, whereas the acidic pathway via **F-I**$_{575}$ is eliminated by the K362M replacement, the reaction of the K362M mutant with peroxide at pH 8.5 does not yield pure **P**$_{607}$ but gives rise to the same mixture of 607 and 580 nm states as observed for WT COX. A second, though less significant, observation is that the 580-type component of intermediate I formed concurrently with the **P**$_{607}$ nm state at pH 8.5 has a peak at 580−582 nm (e.g., Figure 3, inset) rather than at 575 nm.

It is, therefore, reasonable to propose that intermediate I formed in the alkaline pathway is itself a mixture of the 607 and 580 nm states. Accordingly, the generation of two different 580-type **F-I** states formed at alkaline and acidic pH (**F-I**$_{580}$ and **F-I**$_{575}$, respectively) must be considered in addition to the 607 nm intermediate in the phenomenological reaction scheme (see Figure 11 below).

Provisional Reaction Model. A possible scenario of intermediate I formation in the peroxide reaction with the oxidized COX is shown in Figure 11. The scheme proposes that proton uptake via the K-channel is driven by peroxide binding as an initial complex referred to as compound **P**$_0$ followed by heterolytic O−O bond cleavage (*9*). This **P**$_0$ species in which the O−O bond is retained is not observed (also the case in studies of peroxidases, except under specific conditions (*60*)), presumably, because the step after peroxide binding is more rapid. In all 607 and 580 nm-type species that follow this, the O−O bond is considered to the cleaved and the heme a_3 iron to be in ferryl-oxo state. The proposed reaction scheme nicely fits predictions of the eu-oxidase/peroxidase model of the cytochrome oxidase reaction (Figure

1) which postulates the electrogenic transfer of protons via the K-channel coupled to the step of O−O bond cleavage, followed by a transition of the enzyme to the peroxidase conformation and closing the K-channel (*9*, *10*, *19*).

Initially, the oxidized enzyme is in the "eu-oxidase" conformation. The K-channel is open and links the binuclear center with the bulk aqueous phase. Singly (or doubly) ionized hydrogen peroxide binds with heme a_3 forming a transient metastable ferric iron-peroxy adduct, $Fe^{III}-OOH$ (or $Fe^{III}-OO^-$), analogous to compound 0 of peroxidases (hence, the notation $\mathbf{P}_0$ in Figure 11). One proton from H_2O_2 can be consumed to form water if an endogenous hydroxide ligand is expelled from the ferric heme a_3 iron (*24*, *61*). Alternatively, H_2O_2 may deposit a proton(s) on some protein residue either in the input D-channel, as postulated in ref *30*, or in the exit pathway.

Proton-assisted heterolytic cleavage of the O−O bond then abstracts a proton from some internal group(s) on a distal side of heme a_3 (*10*); specific scenarios of such a process have been modeled recently for peroxidases (*11*, *13*) and COX (*12*). Water, the ferryl-oxo $Fe^{IV}=O^{=}$ complex of heme a_3, and a protein radical, probably on the tyrosine residue at the active site, are formed, and a proton vacancy is generated within the site. This proton vacancy is shown, for simplicity, as the generation of OH^- within the heme-copper binuclear center during peroxide cleavage in the alkaline pathway. However, the proton vacancy may be distributed among several interacting acid−base groups within the binuclear center domain (*12*).

The O−O bond scission launches two concurrent processes. The protonic vacancy induced in the binuclear center by peroxide-cleavage (AH, $OH^- \leftrightarrow A^-$, H_2O) pulls in a proton via the K-channel. At the same time, the appearance of a strong oxene ligand at the heme a_3 iron triggers a transition of COX to the peroxidase conformation, and this transition eventually closes the K-channel (*9*, *10*, *19*). As a consequence of this proposed conformational transition, the binuclear center becomes disconnected protonically from the bulk aqueous phase at the level of intermediate I. (A similar proposal has been made independently by Fabian and Palmer in a work (*62*) published after our paper was submitted for publication.) The latter circumstance may provide an alternative (or additional) explanation of the sluggish response of both the $\mathbf{P}_{607}$ and $\mathbf{F\text{-}I}_{575}$ ($F^{\bullet}$) states to pH changes in the medium ((*28*), this work).

In the active COX (WT bacterial or bovine), protonic equilibration of the binuclear center with the bulk aqueous phase via the K-channel may be envisaged to be fast relative to the eu-oxidase → peroxidase conformational transition. Accordingly, at acidic pH, the $\mathbf{P}_{607}$ state in intermediate I fully decays to $\mathbf{F\text{-}I}_{575}$. At alkaline pH, or if proton uptake is inhibited by the K362M replacement, the binuclear center reaches the intermediate I state with one proton less than at acidic pH. This proposal has been corroborated experimentally in a paper (*62*) that appeared after this work was submitted for publication. Under these conditions, as the K-channel closes, an equilibrium mixture of the $\mathbf{P}_{607}$ and $\mathbf{F\text{-}I}_{580}$ states is generated within a closed reaction domain. As indicated in the scheme, the $\mathbf{P}_{607}$ and $\mathbf{F\text{-}I}_{580}$ states may differ by the internal location of a proton. As proposed by several workers, the $\mathbf{P}_{607}$ state may correspond to an OH^- ligand at Cu_B. The protonation of this hydroxide to H_2O,

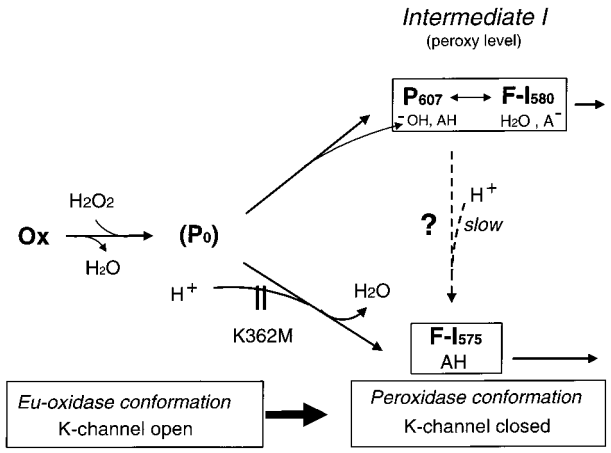

FIGURE 11: A reaction scheme showing the proposed initial products of the reaction of the oxidized *R. sphaeroides* COX with hydrogen peroxide. The enzyme is initially assumed to be in the "eu-oxidase" conformation in which the K-channel is open and connects the binuclear center to the bulk aqueous phase for proton equilibration. The binding and heterolytic scission of hydrogen peroxide is proposed to create a proton deficiency in the binuclear site (denoted as OH^- formation in the scheme). Under acidic conditions, neutralization of this base results in rapid proton uptake prior to the change of the enzyme to the "peroxidase" conformation in which the K-channel is closed. Under alkaline conditions, the proton uptake decelerates (cf. ref *62*) and the K-channel closes prior to protonation of the binuclear site. See the text for further discussion.

either by uptake of a proton (acidic pH-jump experiments) or by redistribution of a proton from an internal donor (AH in Figure 11), converts the $\mathbf{P}_{607}$ intermediate to 580-type absorbing state (*30*, *63*).

Conceivably, internal redistribution of a proton can be associated with redox reequilibration among different groups within the active site. For example, the Cu_B coordination sphere may be considered to have different electron distributions in which an extra oxidizing equivalent is associated either with the tyrosine radical ($^{\bullet}$O-Tyr-His-Cu_B(II)-H_2O) or with trivalent (cupryl) Cu_B (HO-Tyr-His-Cu(III)-OH^-). This type of tautomeric rapid interconversion associated with internal proton movement could be involved in the $\mathbf{P}_{607} \leftrightarrow \mathbf{F\text{-}I}_{580}$ equilibration within the closed binuclear site in the alkaline compound I of COX. Besides, acidic pH may be envisaged to favor reduction of the neutral tyrosine radical to tyrosine by oxidation of a nearby tryptophan, which would form a cation radical (*28*, *33*). Such an intraprotein migration of charge may be a relatively slow process involved in the "spontaneous" decay of the 607 nm state.

The peroxide-independent conversion of the $\mathbf{P}_{607}$ to the $\mathbf{F}_{580}$-type state induced by acid pH-jump (*28*, *62*; this work) is indicated by the dotted line in Figure 11. The process appears to be too slow to imply a specific proton conduction pathway. Moreover, the process is not affected significantly by the K362M or D132N mutations and, hence, may reflect some nonspecific diffusion of H^+ to the closed binuclear site. It is interesting that the final product of the pH 8.5 → pH 6.5 pH-jump with either the WT or K362M COX absorbs not at 575−576 nm, but at 580−581 nm (Figure 8A). Therefore, it is possible that acidification does not convert the alkaline 607 nm species to the acidic $\mathbf{F\text{-}I}_{575}$ ($F^{\bullet}$) species, as considered in refs *28* and *30* and as depicted by the dotted line with a question mark in Figure 11. Rather, the slow

nonspecific leak of protons to the binuclear center may gradually shift the internal equilibrium within the boxed alkaline intermediate I to the **F-I**$_{580}$ state (Figure 11).

A remaining question is why specific (rapid) proton uptake via the K-channel during the formation of intermediate I gives rise to acidic intermediate **F-I**$_{575}$, whereas the **F-I**$_{580}$ form is produced when proton delivery is unspecific (slow) in the course of the acid pH-jump experiment. More direct spectroscopic approaches will be required to elucidate the subtle differences between the 580 and 575 nm ferryl-oxo states that are formed via the alkaline and acidic routes, respectively. One possibility is that these two states differ by the presence or absence of a water molecule at the active site. In the case of rapid proton delivery, water that is formed by the protonation of hydroxide in the binuclear site can exit the heme a_3/Cu$_B$ pocket before the site closes. However, this water molecule may remain trapped in the vicinity of heme a_3 when it is formed as a consequence of slow proton diffusion to the closed binuclear site. The presence of an extra water molecule (or hydroxide) within the closed binuclear site may be sufficient to perturb the structure of the site resulting in the slightly different absorption characteristics (580 vs 575 nm) of the alkaline and acidic ferryl-oxo states. This, of course, is highly speculative, and experiments will be required to clarify the situation.

Input Proton Channels Involved in the Peroxide Reaction. It has been proposed recently that the D-channel controls the pH-dependence of the peroxide reaction with the oxidized COX (*30*). In this model, the reaction via the alkaline route is associated with release of a proton via the D-channel, and the D-channel is involved subsequently in the **P**$_{607}$ → **F-I**$_{575}$ transition (denoted as **P**$_m$ → **F**′ in ref *30*). However, the current data do not reveal an effect of a mutation in the D-channel (D132N) on the initial stage of the peroxide reaction with COX, but provide clear evidence for the involvement of the K-channel in the pH-dependent interplay between the two forms of compound I of COX. The D-channel may be involved, however, in the subsequent H^+-promoted reduction by H_2O_2 of **P**$_{607}$ to **F-II**$_{580}$ in the alkaline pathway (Table 1). Activation of the D-channel at this step, as the K-channel closes, is consistent with the eu-oxidase/peroxidase model (*9*).

The present data are in agreement with the K-channel being involved in the uptake of protons during the reduction of the binuclear site in the oxidized enzyme (*19*, *51*, *64*, *65*). In addition, our results provide a link to a number of earlier observations pointing to vectorial protonation of the binuclear site from the N-aqueous phase. About 30 years ago, the reaction of the oxidized cytochrome oxidase with cyanide was shown to be decelerated severely by the energization of mitochondria (*66*). To explain this striking effect within a framework of Mitchell's chemiosmotic theory, a hypothesis was put forward that the reaction of the heme-copper binuclear center with ionizable ligands is controlled by a proton well involved in electrogenic delivery of the "chemical" protons to the heme a_3 site from the mitochondrial matrix (*67*). As shown in refs *68* and *69*, the energy-dependent inhibition of cyanide binding can be accounted for by a membrane potential-induced deprotonation of a single group with p*K* of ~6.5 at the binuclear center. The group was proposed to be a Cu$_B$ ligand, exchanging protons *electrogenically* with the matrix side of the membrane (*70*). Subsequently, evidence was obtained (*25*) (see also ref *71*) for the involvement of matrix proton(s) in the conversion of the 607 nm state to the 575 nm species during the reaction of the oxidized COX with hydrogen peroxide. The data obtained in the current work suggest that the K-channel is involved in these protonic interactions of the binuclear site with the matrix phase. It can be concluded that in oxidized COX, the protonatable residues buried in the protein in the vicinity of heme a_3 sense the external pH specifically via the K-channel. This is in agreement with the eu-oxidase/peroxidase model of COX mechanism (*9*, *10*).

ACKNOWLEDGMENT

A.K. and R.G. thank Ash Pawate for his kind help during the work on this paper. We gratefully acknowledge stimulating discussion of the results with Joel Morgan, Mikhael Verkhovsky, and Denis Proshlyakov who made relevant observations on bovine COX.

REFERENCES

1. Babcock, G. T., and Wikström, M. (1992) *Nature 356*, 301−309.
2. Ferguson-Miller, S., and Babcock, G. T. (1996) *Chem. Rev. 7*, 2889−2907.
3. Hosler, J. P., Ferguson-Miller, S., Calhoun, M. W., Thomas, J. W., Hill, J., Lemieux, L., Ma, J., Georgiou, C., Fetter, J., Shapleigh, J., Tecklenburg, M. M. J., Babcock, G. T., and Gennis, R. B. (1993) *J. Bioenerg. Biomembr. 25*, 121−136.
4. Fetter, J. R., Qian, J., Shapleigh, J., Thomas, J. W., Garcia-Horsman, A., Schmidt, E., Hosler, J., Babcock, G. T., Gennis, R. B., and Ferguson-Miller, S. (1995) *Proc. Natl. Acad. Sci. U.S.A. 92*, 1604−1608.
5. Iwata, S., Ostermeier, C., Ludwig, B., and Michel, H. (1995) *Nature 376*, 660−669.
6. Ostermeier, C., Harrenga, A., Ermler, U., and Michel, H. (1997) *Proc. Natl. Acad. Sci. U.S.A. 94*, 10547−10553.
7. Tsukihara, T., Aoyama, H., Yamashita, E., Takashi, T., Yamaguichi, H., Shinzawa-Itoh, K., Nakashima, R., Yaono, R., and Yoshikawa, S. (1996) *Science 272*, 1136−1144.
8. Yoshikawa, S., Shinzawa-Itoh, K., Nakashima, R., Yaono, R., Inoue, N., Yao, M., Fei, M. J., Libeu, C. P., Mizushima, T., Yamaguchi, H., Tomizaki, T., and Tsukihara, T. (1998) *Science 280*, 1723−1729.
9. Konstantinov, A. A., Siletskiy, S. A., Mitchell, D., Kaulen, A. D., and Gennis, R. B. (1997) *Proc. Natl. Acad. Sci. U.S.A. 94*, 9085−9090.
10. Konstantinov, A. (1998) *J. Bioenerget. Biomembr. 30*, 121−130.
11. Wirstam, M., Blomberg, M. R. A., and Siegbahn, P. E. M. (1999) *J. Am. Chem. Soc. 121*, 10178−10185.
12. Blomberg, M. R. A., Siegbahn, P. E. M., Babcock, G. T., and Wikstrom, M. (2000) *J. Am. Chem. Soc. 122*, 12848−12858.
13. Filizola, M., and Loew, G. H. (2000) *J. Am. Chem. Soc. 122*, 3599−3605.
14. Proshlyakov, D. A., Pressler, M. A., and Babcock, G. T. (1998) *Proc. Natl. Acad. Sci. U.S.A. 95*, 8020−8025.
15. Babcock, G. T. (1999) *Proc. Natl. Acad. Sci. U.S.A. 96*, 12971−12973.
16. Gennis, R. B. (1998) *Biochim. Biophys. Acta 1365*, 241−248.
17. Konstantinov, A. A., Vygodina, T. V., Capitanio, N., and Papa, S. (1998) *Biochim. Biophys. Acta 1363*, 11−23.
18. Vygodina, T. V., Capitanio, N., Papa, S., and Konstantinov, A. A. (1997) *FEBS Lett. 412*, 405−409.
19. Vygodina, T. V., Pecoraro, C., Mitchell, D., Gennis, R., and Konstantinov, A. A. (1998) *Biochemistry 37*, 3053−3061.
20. Orii, Y. (1982) in *Oxygenases and Oxygen Metabolism* (Nozaki, M., al., e., Eds.) pp 137−149, Academic Press, NY.
21. Orii, Y. (1982) *J. Biol. Chem. 257*, 9246−9248.
22. Vygodina, T. V., and Konstantinov, A. A. (1988) *Ann. NY Acad. Sci. 550*, 124−138.

23. Ksenzenko, M. Y., Berka, V., Vygodina, T. V., Ruuge, E. K., and Konstantinov, A. A. (1992) *FEBS Lett. 297*, 63−66.
24. Konstantinov, A. A., Capitanio, N., Vygodina, T. V., and Papa, S. (1992) *FEBS Lett. 312*, 71−74.
25. Vygodina, T., and Konstantinov, A. (1989) *Biochim. Biophys. Acta 973*, 390−398.
26. Vygodina, T. V., Schmidmaier, K., and Konstantinov, A. A. (1993) *Biol. Membr. (Moscow) 6*, 883−906.
27. Fabian, M., and Palmer, G. (1995) *Biochemistry 34*, 13802−13810.
28. Junemann, S., Heathcote, P., and Rich, P. (2000) *Biochim. Biophys. Acta 1456*, 56−66.
29. Brittain, T., Little, R. H., Greenwood, C., and Watmough, N. J. (1996) *FEBS Lett. 399*, 21−25.
30. Michel, H. (1999) *Biochemistry 38*, 15129−15140.
31. Kitagawa, T., and Ogura, T. (1997) in *Progress in Inorganic Chemistry* (Karlin, K. D., Ed.) pp 431−479, Wiley & Sons, Inc., New York.
32. Fabian, M., Wong, W. W., Gennis, R. B., and Palmer, G. (1999) *Proc. Natl. Acad. Sci. U.S.A. 96*, 13114−13117.
33. Rigby, S. E. J., Junemann, S., Rich, P. R., and Heathcote, P. (2000) *Biochemistry 38*, 5921−5928.
34. MacMillan, F., Kannt, A., Behr, J., Prisner, T., and Michel, H. (1999) *Biochemistry 38*, 9179−9184.
35. Uchida, T., Mogi, T., and Kitagawa, T. (2000) *Biochemistry 39*, 6669−6678.
36. Michel, H., Behr, J., Harrenga, A., and Kannt, A. (1998) *Annu. Rev. Biophys. Biomol. Struct. 27*, 329−356.
37. Wikstrom, M., Morgan, J. E., and Verkhovsky, M. (1998) *J. Bioenerget. Biomembr. 30*, 139−145.
38. Brzezinski, P., and Adelroth, P. (1998) *J. Bioenerget. Biomembr. 30*, 99−107.
39. Ruitenberg, M., Kannt, A., Bamberg, E., Ludwig, B., Michel, H., and Fendler, K. (2000) *Proc. Natl. Acad. Sci. U.S.A. 97*, 4632−4636.
40. Moody, A. J. (1996) *Biochim. Biophys. Acta 1276*, 6−20.
41. Bergmayer, H. U., Gawehn, K., and Grassl, M. (1970) in *Methoden der Enzymatischen Analyze* (Bergmayer, H. U., Ed.) p 440, Verlag Chemie, Weinheim.
42. Mitchell, D. M., and Gennis, R. B. (1995) *FEBS Lett. 368*, 148−150.
43. Henry, E. R., and Hofrichter, J. (1992) *Methods Enzymol. 210*, 129.
44. Maeder, M., and Zuberbuhler, A. (1990) *Anal. Biochem. 62*, 2220.
45. Gorren, A. C. F., Dekker, H., and Wever, R. (1986) *Biochim. Biophys. Acta 852*, 81−92.
46. Weng, L., and Baker, G. M. (1991) *Biochemistry 30*, 5727−5733.
47. Wikström, M., Krab, K., and Saraste, M. (1981) *Cytochrome Oxidase − A Synthesis*, Academic Press, New York.
48. Rich, P., and Moody, A. J. (1997) in *Bioenergetics* (Graber, P., and Milazzo, G., Eds.) pp 419−456, Birkhauser.
49. Nicholls, P., and Chanady, G. A. (1981) *Biochim. Biophys. Acta 634*, 256−265.
50. Fabian, M., and Malmström, B. G. (1989) *Biochim. Biophys. Acta 973*, 414−419.
51. Junemann, S., Meunier, B., Gennis, R. B., and Rich, P. (1997) *Biochemistry 36*, 14456−14464.
52. Mills, D. A., and Ferguson-Miller, S. (1998) *Biochim. Biophys. Acta 1365*, 46−52.
53. Vygodina, T. V., and Konstantinov, A. A. (1987) *FEBS Lett. 219*, 387−392.
54. Gorren, A. C. F., Dekker, H., Vlegels, L., and Wever, R. (1988) *Biochim. Biophys. Acta 932*, 277−286.
55. Orii, Y. (1988) *Ann. NY Acad. Sci. 550*, 105−117.
56. Bickar, D., Bonaventura, J., and Bonaventura, C. (1982) *Biochemistry 21*, 2661−2666.
57. Wrigglesworth, J. (1984) *Biochem. J. 217*, 715−719.
58. Wrigglesworth, J. M., Elsden, J., Chapman, A., Van der Water, N., and Grahn, M. F. (1988) *Biochim. Biophys. Acta 93*, 452−464.
59. Witt, D. N., and Chan, S. I. (1987) *J. Biol. Chem. 262*, 1446−1448.
60. Baek, H. K., and Van Wart, H. E. (1989) *Biochemistry 28*, 5714−5719.
61. Zaslavsky, D., Smirnova, I. A., Adelroth, P., Brzezinsky, P., and Gennis, R. B. (1999) *Biochemistry 38*, 2307−2311.
62. Fabian, M., and Palmer, G. (2001) *Biochemistry 40*, 1867−1874.
63. Wikstrom, M. (2000) *Biochim. Biophys. Acta 1458*, 188−198.
64. Kannt, A., Lancaster, C. R. D., and Michel, H. (1998) *Biophys. J. 74*, 708−721.
65. Wikstrom, M. K. F., Jasaitis, A., Backgren, C., Puustinen, A., and Verkhovsky, M. I. (2000) *Biochim. Biophys. Acta 1459*, 514−520.
66. Wilson, D. F., and Fairs, K. (1974) *Biochim. Biophys. Res. Commun. 56*, 635−640.
67. Konstantinov, A. A. (1977) *Doklady Akad. Nauk SSSR 237*, 713−716.
68. Andreev, I. M., Artzatbanov, V. Y., Konstantinov, A. A., and Skulachev, V. P. (1979) *Dokl. Acad. Nauk SSSR 244*, 1013−1017.
69. Andreev, I. M., and Konstantinov, A. A. (1983) *Bioorg. Chem. (Moscow) 9*, 216−227.
70. Konstantinov, A. A., Vygodina, T. V., and Andreev, I. M. (1986) *FEBS Lett. 202*, 229−234.
71. Wikström, M. (1988) *FEBS Lett. 231*, 247−252.

BI010115V